Water Resources Research

RESEARCH ARTICLE
10.1029/2023WR036727

Determining the Relative Contributions of Runoff, Coastal, and Compound Processes to Flood Exposure Across the Carolinas During Hurricane Florence

Lauren E. Grimley[1], Antonia Sebastian[1], Tim Leijnse[2,3], Dirk Eilander[2,4], John Ratcliff[1,5], and Rick Luettich[1,5]

[1]Department of Earth, Marine and Environmental Sciences, University of North Carolina at Chapel Hill, Chapel Hill, NC, USA, [2]Institute for Environmental Studies (IVM), Vrije Universiteit Amsterdam, Amsterdam, The Netherlands, [3]Department of Marine and Coastal Systems, Deltares, Delft, The Netherlands, [4]Department of Inland and Water Systems, Deltares, Delft, The Netherlands, [5]UNC Institute of Marine Sciences, Morehead City, NC, USA

Abstract Estimates of flood inundation generated by runoff and coastal flood processes during tropical cyclones (TCs) are needed to better understand how exposure varies inland and at the coast. While reduced-complexity flood models have been previously shown to efficiently simulate TC flood processes across large regions, a lack of detailed validation studies of these models, which are being applied globally, has led to uncertainty about the quality of the predictions of inundation depth and extent and how this translates to exposure. In this study, we complete a comprehensive validation of a hydrodynamic model (SFINCS) for simulating pluvial, fluvial, and coastal flooding. We hindcast Hurricane Florence (2018) flooding in North and South Carolina, USA using high-resolution meteorologic data and coastal water level output from an ocean recirculation model (ADCIRC). Modeled water levels are compared to traditional validation datasets (e.g., water level gages, high water marks) as well as property-level records of insured flood damage to draw conclusions about the model's performance. SFINCS shows skill in simulating runoff and coastal processes of TC flooding (peak error of 0.11 m with an RMSE of 0.92 m) at large scales with minimal computational requirements and limited calibration. We use the validated model to attribute flood extent and building exposure to flood processes (e.g., runoff, coastal, compound) during Hurricane Florence. The results highlight the critical role runoff processes have in TC flood exposure and support the need for broader implementation of models capable of realistically representing the compound effects resulting from coastal and runoff processes.

Plain Language Summary This study focuses on improving our understanding of hurricane flood risk. We use an inundation model to simulate flooding caused by Hurricane Florence (2018) in North and South Carolina, USA. The accuracy of the model is assessed by comparing modeled water levels to measurements taken in the field and records of property-level damage. We find that the model can accurately simulate hurricane flooding, including storm surge and rainfall, across large regions (e.g., watersheds) with minimal computational requirements and limited calibration. We use the model to analyze flood extent and building exposure during Hurricane Florence, attributing them to runoff and coastal processes. The results emphasize the significant role that rainfall plays in hurricane flood exposure and the need for models capable of representing flooding from both processes.

Key Points:

- SFINCS reproduces observations of flooding from Hurricane Florence from 0 to 80 m + NAVD88 with an average peak error of 0.11 m
- Modeled inundation covered 14,301 sq. km. of the Carolinas where runoff processes contributed the majority (55%) of building exposure
- Nonlinear, compound processes account for 15% of total inundation, exacerbating water levels on average by 0.1 m at 31% of exposed buildings

Supporting Information:

Supporting Information may be found in the online version of this article.

Correspondence to:

L. E. Grimley,
lauren.grimley@unc.edu

Citation:

Grimley, L. E., Sebastian, A., Leijnse, T., Eilander, D., Ratcliff, J., & Luettich, R. (2025). Determining the relative contributions of runoff, coastal, and compound processes to flood exposure across the Carolinas during Hurricane Florence. *Water Resources Research*, *61*, e2023WR036727. https://doi.org/10.1029/2023WR036727

Received 14 NOV 2023
Accepted 28 FEB 2025
Corrected 4 APR 2025

This article was corrected on 4 APR 2025. See the end of the full text for details.

Author Contributions:

Conceptualization: Lauren E. Grimley, Antonia Sebastian, Rick Luettich
Data curation: Lauren E. Grimley
Formal analysis: Lauren E. Grimley
Funding acquisition: Antonia Sebastian, Rick Luettich
Investigation: Lauren E. Grimley
Methodology: Lauren E. Grimley
Resources: Tim Leijnse, John Ratcliff

1. Introduction

Tropical Cyclones (TCs) generate widespread flooding that can lead to damages on the order of thousands of millions of US dollars (NCEI, 2023). TC flooding is influenced by multiple drivers including mean sea level (MSL), storm tide (e.g., surge), waves, wind, rainfall, and streamflow (Gori et al., 2022; Lai et al., 2021). Evidence suggests that TC-related flood damages are increasing in response to changes in TC characteristics and sea level rise (Meiler et al., 2022; Strauss et al., 2021), as well as development in coastal areas (Hallegatte et al., 2013; Hoeppe, 2016; Klotzbach et al., 2018; Merkens et al., 2016; Pörtner et al., 2023). For example, global annual costs associated with TCs tripled between 1990 and 2021 (Klotzbach et al., 2022) where the frequency of the most damaging storms is increasing at a higher rate than moderately damaging storms (Grinsted et al., 2019). Despite the rising costs associated with TCs, comprehensive flood exposure assessments are lacking, as most previous studies neglect to assess the full extent of flood inundation from TCs, instead focusing on modeling individual flood drivers and their associated processes (e.g., storm surge or rainfall-runoff) at large scales because the models

Software: Lauren E. Grimley, Tim Leijnse, Dirk Eilander
Supervision: Antonia Sebastian
Validation: Lauren E. Grimley
Visualization: Lauren E. Grimley
Writing – original draft: Lauren E. Grimley
Writing – review & editing: Lauren E. Grimley, Antonia Sebastian, Tim Leijnse, Dirk Eilander, John Ratcliff, Rick Luettich

do not resolve the relevant physics (Bakhtyar et al., 2020; Colle et al., 2008; Dietrich et al., 2011; Ray et al., 2011; Torres et al., 2015), or compound flood processes at smaller scales because the models are too computationally expensive (e.g. Gori, Lin, & Xi, 2020; Q. Liu et al., 2022; Loveland et al., 2021; Maymandi et al., 2022; Xu et al., 2022; Zhang et al., 2020).

TC flooding can extend far beyond the coastline and landfall location as a result of rainfall-runoff and compound processes that drive flood inundation (Kunkel & Champion, 2019; Titley et al., 2021). Increasingly, flood modelers are using reduced-physics solvers, subgrid options, and downscaling methods to overcome computational challenges associated with large scale (e.g., regional, continental, global) flood modeling (Leijnse et al., 2021; Neal et al., 2012, 2018; Sanders & Schubert, 2019; Schumann et al., 2014). Yet, there are relatively few in-depth validations of reduced-complexity performance spanning pluvial, fluvial, and coastal transitions (Bates et al., 2021a; Nederhoff et al., 2024; Wing et al., 2017, 2021), and given growing public interest in using them in both planning and forecasting applications, there is a need for robust assessment of their performance increase trust in their application for flood exposure (Bates, 2021; Schubert et al., 2024; Trigg et al., 2016).

In this study, we address two gaps: a lack of comprehensive assessment of TC flood exposure and need for more robust validation studies of existing models. We conduct a detailed and transparent evaluation of a reduced-complexity model Super-Fast INundation of CoastS (SFINCS) for simulating pluvial, fluvial, and coastal flooding from Hurricane Florence, contributing to a representative sample of model validation studies. The SFINCS model was developed with limited calibration, instead using the best available topobathymetric data and forced with high-resolution hydrometeorological data. SFINCS is one-way coupled to ADvanced CIRCulation (ADCIRC) model at the coastal boundary (see Santiago-Collazo et al. (2019) for a review of compound inundation models and coupling approaches). Whereas previous studies of Hurricane Florence have focused on assessing model performance at a single site (Gori, Lin, & Smith, 2020) or comparing model outputs to observational data typically below 20 m + NAVD88 (Bao et al., 2022; Nederhoff et al., 2023; Ratcliff, 2022; Ye et al., 2021), we complete a comprehensive assessment of the full extent of flooding from inland (up to 200 m + NAVD88) to the coast across a large portion of North (NC) and South Carolina (SC) (referred to as the Carolinas). Modeled water levels were validated against point-level observations of flood inundation, including water level measurements at gages, high-water marks (HWMs), and property-level records of flood exposure. We use the model to comprehensively assess building exposure in the Carolinas, attributing it to coastal, runoff, and compound processes far beyond the storm's landfall location. We demonstrate that our modeling approach provides an accurate assessment of TC flooding both inland and at the coast making it useful for future planning and forecasting applications.

2. Background

The study area (78,007 sq. km.) encompasses portions of five USGS Hydrologic Unit Code (HUC) 6-digit watersheds spanning the Carolinas including the Lower Pee Dee (LPD), Cape Fear (CF), Onslow Bay (OB), Neuse (N), and Pamlico (P) watersheds (Figure 1). This area experiences TC landfall on average every 5–8 years (NOAA & NHC, 2023). Notable historical hurricanes include Fran (1996), Floyd (1999), Matthew (2016), Florence (2018), and Dorian (2019). Of these, Hurricane Florence provides a uniquely large dataset against which to validate inundation models. Florence made landfall as a Category 1 storm near Wilmington, NC on 14 September 2018, and generated record-setting flooding across the two States (Hall & Kossin, 2019; Kunkel & Champion, 2019). The highest land-based sustained winds averaged 79 kt (40.6 m/s), maximum storm surge heights across the Carolinas ranged between 0.9 and 3.4 m above MSL and rainfall totals ranged from 254 to 913 mm (Stewart & Berg, 2019). After landfall, Florence weakened and slowly moved farther inland across SC generating heavy rainfall over 2–4 days. Damages exceeded 2 billion US dollars (FEMA, 2020).

3. Methods

3.1. Hydrodynamic Model

We used the Super-Fast INundation of CoastS (SFINCS), a two-dimensional hydrodynamic model, that uses reduced-complexity solvers to simulate multiple drivers of flooding at the river-coastal interface (Leijnse et al., 2021). SFINCS uses a structured grid and accounts for spatially varying rainfall, infiltration, overland roughness, wind and atmospheric pressure. An advantage of SFINCS over other models is that it runs "super-fast" because it computes overland flow using simplified equations of mass and momentum with an adaptive timestep.

10.1029/2023WR036727

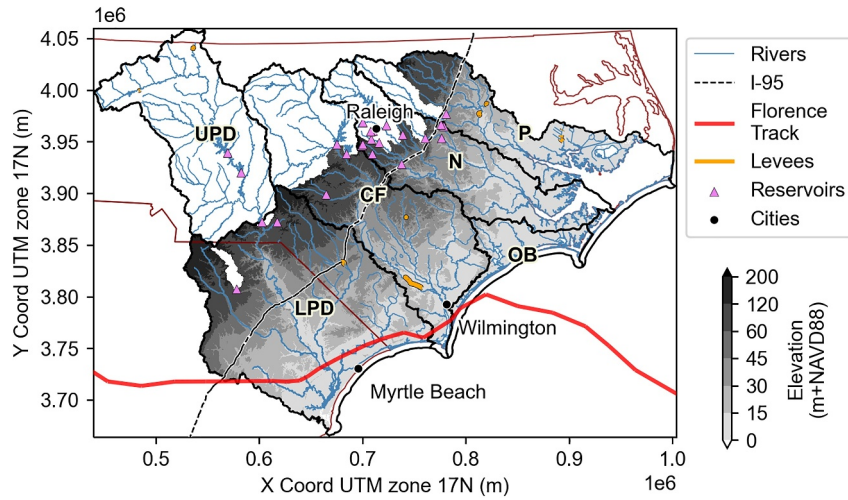

Figure 1. The study area includes five USGS HUC6 watersheds in North and South Carolina (boundaries outlined in dark red) including the Lower Pee Dee (LPD), Cape Fear (CF), Neuse (N), Onslow Bay (OB), and Pamlico (P) which are outlined in black. The relative size of the Upper Pee Dee (UPD) basin which drains into the LPD is shown. Elevations in meters above the North American Vertical Datum of 1988 (NAVD88) are shown for the area included in the SFINCS model domain. Large reservoirs where river discharge is controlled are denoted as pink triangles. For context, the location of Wilmington and Raleigh, NC as well as Myrtle Beach, SC are shown in black dots. Hurricane Florence's storm track is a solid red line, Interstate 95 (I-95) is a dashed black line, and major levees are solid orange lines.

SFINCS uses a subgrid method (e.g., see similar methods developed by Casulli (2009) and Volp et al. (2013)) to account for bed level and roughness variations on a smaller scale than the native model grid, enabling it to have increased computational speed without sacrificing model accuracy (Leijnse et al., 2020). SFINCS is built using open-source and open-access tools (Eilander, Boisgontier, et al., 2023; Eilander et al., 2022) making it easily replicated in new areas (van Oosterhout et al., 2023).

SFINCS has been widely applied to simulate flooding in urban, coastal environments (Sebastian et al., 2021), large watersheds (Eilander, Couasnon, Leijnse, et al., 2023; Eilander, Couasnon, Sperna Weiland et al., 2023), and coastlines (Nederhoff et al., 2023). However, prior evaluations of model performance have primarily focused on comparing SFINCS outputs to observations below 20 m + NAVD88 or to other, more computationally expensive hydrodynamic models (e.g., XBeach; Bertoncelj et al. (2021) and Delft3D FM; Röbke et al., 2021)). We add to these previous studies with a detailed evaluation of SFINCS for simulating total water levels generated by both coastal and runoff processes, with a specific focus on the model's accuracy for pluvial and fluvial applications at locations further inland.

3.2. Model Setup

The SFINCS grid was constructed with a spatial resolution of 200 m and contains over 1.95 million cells. Property tables at the subgrid resolution of 5.0 m—1/40th of the computational grid resolution—were generated using high-resolution elevation and land cover data. Several topographic and bathymetric DEMs were used to assign the elevation data used in the model including a USGS Coastal National Elevation Dataset (CoNED), USGS National Elevation Dataset (NED), LiDAR-derived DEMs for NC, and analyzed bathymetry data exported from river models. The final elevation raster used in the SFINCS model is described in more detail in Supporting Information S1 and is available for download from DesignSafe https://doi.org/10.17603/ds2-mzc8-s589 (Grimley & Sebastian, 2025). Overland roughness values were assigned using a modified version of the National Land Cover Data (NLCD) 2016 Land Cover Product (Figure S5 in Supporting Information S1) and average values for the Manning's n friction coefficients that are within the range of plausible values (Table S1 in Supporting Information S1) (Chow et al., 1998; Z. Liu et al., 2019; Savage et al., 2016). Spatially varying infiltration was simulated in SFINCS using the Soil Conservation Services (SCS) Curve Number (CN) Loss Model with recovery (EPA, 2015; USDA-NRCS, 2004). CNs were assigned using 30 m rasters of land cover data and soil-related data from the Gridded National Soil Survey Geographic (gNATSGO) Database (Soil Survey Staff, 2022) (Table S2 in Supporting Information S1). 44 km of levees from the National Levee Database (NLD) were included in the

model as weirs (weir coefficient of 0.6) and crest elevations were extracted from the DEM. Additional information on the model setup are described in more detail in the Supplemental Materials.

Analyzed and observed data was input to the model to simulate 23-day of total water levels during Hurricane Florence (September 7–30, 2018). Initial soil moisture conditions were set to 75% of the maximum capacity and the initial water level at the coast was set to 0.25 m + NAVD88. A 24-hr startup period was applied to allow the coastal water level to stabilize, filling the bays and estuaries with water. Discharge, coastal water level, rainfall, and wind inputs are applied to the model starting 7 days prior to Hurricane Florence landfall (14 September 2018). NOAA's Multi-Radar Multi-Sensor (MRMS) Quantitative Precipitation Estimate (QPE) gridded rain-gage adjusted, radar-rainfall data which has a spatial resolution of 1.0 km and temporal resolution of 1-hr (the total rainfall for the entire simulation is shown in Figure S6 in Supporting Information S1). Nine discharge time series from USGS gages with a 15-min temporal resolution (Figure S2 and Figure S3 in Supporting Information S1) were applied at the upstream boundary of the model and 20-min water levels (storm tide) simulated using a previously validated ADCIRC model for Hurricane Florence (see Ratcliff, 2022) were applied at the downstream boundary of the model. Both ADCIRC and SFINCS were forced with re-analyzed wind fields that are a modified version of the proprietary Ocean Weather Inc. (OWI) which has a spatial resolution of 0.05-degree (~5.0 km) and a 15-min temporal resolution (maximum wind speeds are shown in Figure S6 in Supporting Information S1). Wind drag coefficients applied to the model varied linearly from 0.001 to 0.0025 between wind speeds of 0–28 m/s and then remains constant at 0.0025 for wind speeds greater than 28 m/s (Garratt, 1977). Note, the wind files were only available for the first 11 days of the simulation period, after this, no wind was applied to the grid.

3.3. Performance Metrics

We performed a detailed assessment of the model performance across the study area comparing modeled and observed water levels at gages and high water marks (HWMs), and flood depths to property-level records of insured damage.

3.3.1. Water Levels and Depths

Three metrics were considered for the timeseries comparison at gages: Bias (also known as the Mean Error), Root-Mean-Square-Error (RMSE), and the Coefficient of Determination, and an additional metric: Peak Error (PE), was considered when comparing water levels recorded at both gages and HWMs. The Bias quantifies whether the model tends to under or overpredict the observed water levels across the simulation; the RMSE quantifies the absolute deviations between modeled and observed water levels (i.e., the spread) noting that the RMSE highlights large errors; and the Coefficient of Determination measures the "goodness-of-fit" between model simulations and observations (Krause et al., 2005). The Coefficient of Determination estimates the combined dispersion to the individual dispersion of the modeled and observed data where a value of zero indicates poor model performance and a higher value is associated with good model performance. While the Coefficient of Determination is not a perfect measure and does not indicate whether there is a systematic bias meaning it can be low for an accurate model or high for an inaccurate model, it is widely used for estimating the predictive ability of the model to replicate measured water levels (Jackson et al., 2019) and therefore included in this study. These performance metrics were calculated at 89 permanent water level gages that had at least 50 measurements during the simulation period using all available observational data for the entire 23-day simulation including normal flow conditions, even if the station had data gaps or missed the peak flood. PE is a useful indicator of peak flood extent which is important for estimating exposure and damage. PE in the modeled water level was calculated at the 89 permanent water level gages and at 763 HWMs that had a quality greater than "Fair:±0.12 m". Flood depth grids were created for each scenario by downscaling modeled water levels based on a higher resolution terrain of 20 m, excluding those below 0.05 m. We compared the modeled depths to the depths reported at 476 USGS HWM locations.

3.3.2. Property-Level Building Exposure

Property-level data on Federal Insurance and Mitigation Administration (FIMA) National Flood Insurance Program (NFIP) policies and claims during Hurricane Florence (selected dates of September 6–30, 2018; see Thomson et al. (2023) for a description of the data) were used to generate a contingency matrix to assess how well the model predicts flood exposure at buildings in NC (i.e., where reported damage or no damage serves as a proxy

for exposure). We extract modeled water depths at 22,858 buildings (1.5% of the total buildings within the NC portion of the model domain, n = 1,488,229) where 11,073 buildings were associated with a NFIP claim and 11,785 buildings were associated with a NFIP policy but no claim.

Forecast verification metrics generated from the contingency matrix were first employed to indicate the value of flood warning (Schaefer, 1990) and more recently for modeled flood extent to other model output (Bates et al., 2021b) or remotely sensed flood extents (Courty et al., 2017). The contingency matrix includes true positives (TP), false positives (FP), true negatives (TN), and false negatives (FN) calculated using a flood depth threshold. The number of events is equal to the total number of buildings that reported damage (i.e., E = TP + FP) and the total number of cases is equal to the events and the total number of buildings that reported no damage (i.e., C = E + TN + FN). When the model predicts flooding above a specified depth threshold at a building that is associated with a claim, it was considered a true positive. Conversely, a false positive occurs when the model does not predict flooding at a building where a claim was filed. A building might also be associated with a policy but not a claim suggesting that the building did not experience flooding. A false negative occurs when the model predicts flooding at a building that had a policy but was not associated with a claim. A true negative occurs when the model did not predict flooding at a building that had a policy but not a claim. The following statistics were calculated.

- Accuracy is the fraction of the modeled flooded and non-flooded locations that were correctly predicted where Accuracy = (TP + TN)/C.
- Bias measures the ratio of the frequency of modeled flooded locations to the frequency of observed damaged locations where Bias = (TP + TN)/E) - 1. A tendency to underpredict is BIAS <0 while a tendency to overpredict is BIAS >0.
- Probability of Detection (POD), also known as hit rate, is the fraction of modeled flooded locations (e.g., true positives) that were correctly predicted where POD = TP/E. This score does not penalize for false negatives.
- False Alarm Ratio (FAR) is the fraction of modeled flooded locations that were not correctly predicted (e.g., no damage reported) where FAR = FN/(TN + FN).
- Success Ratio (SR) is the fraction of the modeled flooded locations that were observed where SR = TP/(TP + TN).
- The Critical Success Index (CSI) measures the ratio of the modeled flooded locations to the observed where CSI = TP/(E+ TN). The CSI is sensitive to the number of true positives and penalizes both the false positives and false negatives.

3.4. Sensitivity Analysis

A sensitivity analysis was conducted as a form of calibration of the model where performance metrics for varying grid resolution, varying channel complexity in the terrain, antecedent soil conditions, and roughness values were compared. In addition, we tested the influence of grid resolution on computational time. While an in-depth sensitivity analysis of the model performance for different inputs was not the focus of this study, performance metrics for several tests are provided in Table S3 to Table S6 and Figure S7 in Supporting Information S1.

3.5. Flood Process Attribution

We simulated flooding caused by each of the individual flood drivers (i.e., river discharge, rainfall, wind, storm tide). Then, we attributed peak flood depth and inundation extent to (a) runoff processes where we applied river discharge, rainfall, and a constant coastal water level (b) coastal processes where we applied ADCIRC coastal water level (storm surge and tides), and wind forcings, and (c) compound scenario where all forcings are applied. Inundation was attributed to compound processes when the water level in the compound scenario exceeded water levels from either of the two individual scenarios by at least 0.05 m. If the compound simulation did not generate water levels greater than 0.05 m, peak water level drivers were attributed to the individual runoff or coastal processes, whichever simulation generated a larger water level. This simplified approach has been used in other studies with thresholds ranging between 0.01 and 0.2 m (Eilander, Couasnon, Leijnse, et al., 2023; Gori, Lin, & Xi, 2020; Shen et al., 2019). The compound extent we identify might be slightly larger than the "transition zone" which Bilskie and Hagen (2018) defines as the area where the rainfall-runoff simulations generate water levels less than the storm tide simulation, but neither is dominant compared to the simulation of them combined.

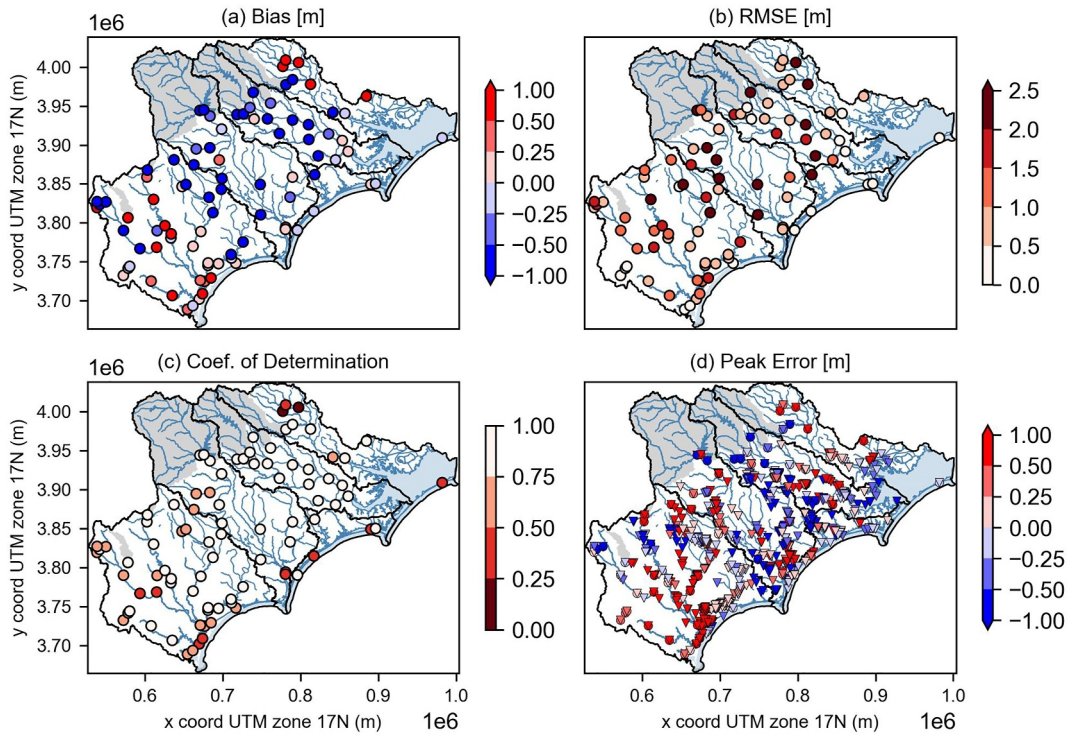

Figure 2. (a) Bias (m), (b) Root-Mean-Square-Error (RMSE) (m), (c) Coefficient of Determination, and (d) Peak Error (m) at 89 water level gages (circles) and 763 high water marks (HWMs) (triangles).

After attributing inundation to the three processes, we estimate the total area of overland impact, excluded areas within the major coastal water bodies and estuaries (see Figure S1 in Supporting Information S1) from the calculation. The calculated runoff, coastal, and compound extents were used to assign building exposure. To do this we used the National Structure Inventory (NSI) maintained by the USACE in SC (n = 428,051) and building footprints available from North Carolina Emergency Management (NCEM) in NC (n = 1,488,229). There are 472,089 buildings in the Cape Fear; 660,780, in the Lower Pee Dee; 379,586 in the Neuse; 199,696 in Onslow Bay, and 200,523 in the Pamlico basins. At the building centroids, we extracted elevation data from the model subgrid DEM (e.g., 5 m resolution) and subtracted modeled peak water levels to get depths associated with runoff, coastal, and compound scenarios.

4. Results

4.1. Model Performance

4.1.1. Water Levels and Depths

We compared the model performance to water level measurements at 89 individual gages and 763 high-water mark locations across the domain (Figure 2), and summarize performance metrics by HUC6, state, and for the entire domain (Table 1). When compared to observed hydrographs, the model has an average bias of −0.32 m, an RMSE of 1.20 m, and a Coefficient of Determination of 0.77. The average peak water level error across the domain is 0.11 m and the RMSE of these peak errors is 0.92 m (Figure 3). Modeled depths relative to the SFINCS subgrid were compared to the depths recorded in the USGS HWM data (Figure 3). The average peak depth error across the domain is 0.25 m and the RMSE of these peak errors is 0.97 m. This suggests that overall, the model is unbiased; however, when considering the spatial pattern of these errors, Figure 2d demonstrates that the model tends to underpredict water levels in NC but overpredict water levels in SC. In the Supplemental Materials, we include a larger plot of the peak errors in Figure 2d (Figure S8 in Supporting Information S1), performance metrics per USGS gage (Table S7 in Supporting Information S1), modeled hydrographs compared to USGS stages (Figure S9 in Supporting Information S1), and the empirical distribution of model peak error (m) (Figure S10 in Supporting Information S1).

Table 1
Modeled Hydrographs Were Compared to Gage Observations Using Statistics of the Bias, Root-Mean-Square-Error (RMSE), and Coefficient of Determination Which Were Calculated Across the 23-Day Simulation

		Hydrograph			Peak water level	
Performance metric		Bias (m)	RMSE (m)	Coeff. Of Det.	Bias (m)	RMSE (m)
HUC6	Cape Fear	−0.88	1.71	0.81	0.04	1.22
	Lower Pee Dee	−0.08	1.13	0.75	0.35	0.89
	Neuse	−0.92	1.23	0.88	−0.08	0.72
	Onslow Bay	−0.40	0.61	0.68	−0.19	0.67
	Pamlico	0.56	1.07	0.65	0.06	0.48
Region	NC	−0.62	1.34	0.80	−0.03	0.90
	SC	0.16	1.04	0.72	0.61	0.98
	Domain	−0.32	1.20	0.77	0.11	0.92

Note. Peak water level bias and RMSE were compared to observed peaks at gages and HWM locations. Metrics were averaged across each HUC6 watershed, state, and for the entire domain.

4.1.2. Property-Level Building Exposure

We classified buildings as flooded or not flood using six depth thresholds. Across all depth thresholds, the model correctly predicts flooding at 67% (POD) of the building locations that reported damage (n = 11,073) which reflects the model's tendency to underpredict the number of flooded locations (bias <0) even at the lowest depth threshold (Table 2). The fraction of the modeled flooded locations that were correctly observed was 0.84–1.0 (SR), increasing with larger depth thresholds. The highest model accuracy occurs when using a depth threshold of 1.5 m. The model correctly predicts 84% of the cases (n = 22,858) of damage and no damage and has the best CSI score of 0.67 and a low FAR of 1%. However, the model still has a large bias of −0.32.

4.2. Flood Process Attribution

4.2.1. Water Levels and Peak Flood Extent

The peak flood extent (excluding coastal water bodies and estuaries) was 14,301 sq. km. (18.3% of the domain), where runoff processes account for 79.2% (11,320 sq. km.), coastal processes account for 5.9% (842 sq. km.) and compound processes account for 15.3% (2,140 sq. km.) of the inundation within the model domain (Figure 4a). Compound processes increased peak water levels on average by 0.11 m (95% Confidence Interval (CI): 0.05–0.25 m) compared to the maximum of the individual coastal or runoff processes (Figure 4b). Areas that experienced the greatest increase in water level due to the combination of flood processes were primarily below 20 m + NAVD88; however, compound flooding did not always lead to higher water levels (blue areas in Figure 4b). The peak flood depth is shown in Figure S12 in Supporting Information S1 and the contribution of the individual model forcings (e.g., wind, rainfall, discharge, storm tide) to peak water levels are shown in Figure S13 in Supporting Information S1.

4.2.2. Building Exposure

Hurricane Florence exposed 75,341 buildings (3% of total across the domain) to at least 0.15 m (0.5 ft) of inundation where runoff, coastal, and compound processes led to exposure at 55%, 14%, and 31%, respectively (Figure 5). Across the domain, the mean depth at buildings due to runoff processes was 1.07 m (95% CI: 0.19–3.29 m), to coastal processes was 0.66 m (95% CI: 0.18–1.35 m), and to compound processes was 0.80 m (95% CI: 0.20–1.77 m). Runoff processes contributed to most of the building exposure in the Lower Pee Dee and the Cape Fear. Approximately 96% and 95% of buildings, respectively, were exposed to runoff processes with mean depths of 0.99 and 1.47 m. While coastal processes were the primary driver of building exposure in Onslow Bay (66%) with mean depths of 0.71 m (95% CI: 0.20–1.43 m), runoff processes generated greater depths on average (mean of 0.77 m with 95% CI: 0.17–2.05 m). Compound processes contributed to most of the building exposure in the Neuse and Pamlico: 71% and 83%, respectively. The mean depths due to compound processes were 0.88 m (95% CI: 0.22–1.87 m) in the Neuse and 0.70 m (95% CI: 0.20–1.58 m) in the Pamlico. Using a larger depth threshold

10.1029/2023WR036727

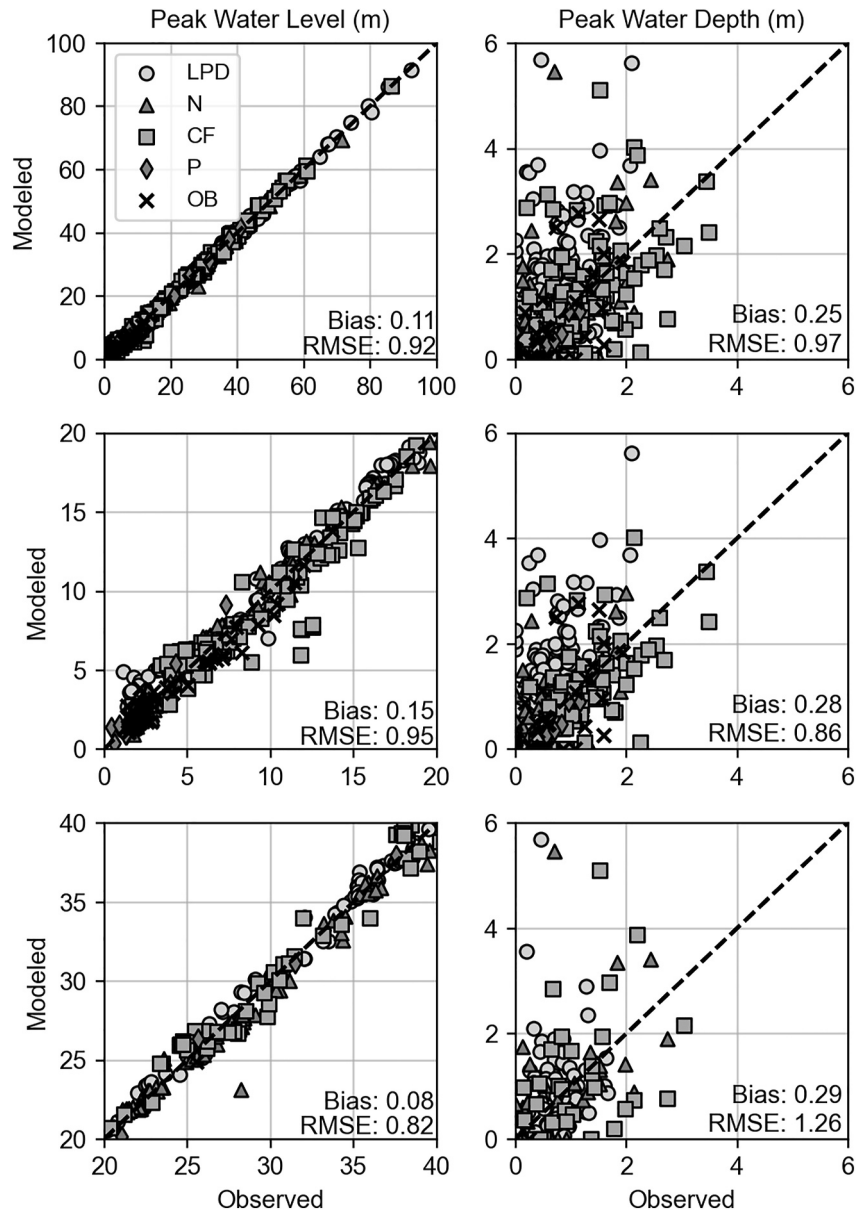

Figure 3. Observed and modeled peak water levels were compared at 763 High Water Mark (HWM) locations and 89 water level gages across the five HUC6 watersheds: Lower Pee Dee (LPD), Neuse (N), Cape Fear (CF), Pamlico (P), and Onslow Bay (OB). The first column compares the observed and predicted water levels and the second column compares water depths at 476 USGS HWM locations. We compare the depth data reported in the USGS HWM to the modeled depths relative to the subgrid. The QQ-plots show this comparison at all locations (top row), those with elevations ≤20 m + NAVD88 (middle row), and those with elevations between 20 and 40 m + NAVD88 (bottom row). The 1:1 line is also plotted and the model bias and RMSE for the data shown in each subplot is listed in the bottom right corner.

would reduce the number of exposed buildings; for example, we estimate that 23,630 buildings were exposed to flood depths greater than 1.0 m where runoff, coastal, and compound processes contributed 66%, 7%, and 27% of building exposure, respectively (see Figure S14 in Supporting Information S1).

Compound processes exacerbate maximum water levels at exposed buildings by 0.10 m on average (95% CI: 0.06–0.21 m) (Figure 6a). The median is only slightly lower at 0.09 m. Buildings in Onslow Bay experienced the largest effect of compound processes as peak water levels increased on average by 0.13 m (95% CI: 0.05–0.45 m) relative to either runoff or coastal processes. The maximum amplification of water levels due to compound processes at any individual building was 0.19, 0.85, 1.69, 1.88, and 2.03 m in the Cape Fear, Lower Pee Dee,

Table 2
Forecast Verification Metrics Calculated Using the Contingency Matrix of True Positives, False Positives, True Negatives, and False Negatives for Six Depth Thresholds

Forecast verification metric	Perfect score	Flood depth threshold (m)					
		0.05	0.1	0.5	1.0	1.5	2.0
Accuracy	1	0.78	0.78	0.81	0.83	0.84	0.84
Bias	0	−0.20	−0.21	−0.27	−0.31	−0.32	−0.33
POD	1	0.67	0.67	0.67	0.67	0.67	0.67
FAR	0	0.16	0.15	0.08	0.03	0.01	0.00
SR	1	0.84	0.85	0.92	0.97	0.99	1.00
CSI	1	0.59	0.60	0.63	0.65	0.67	0.67

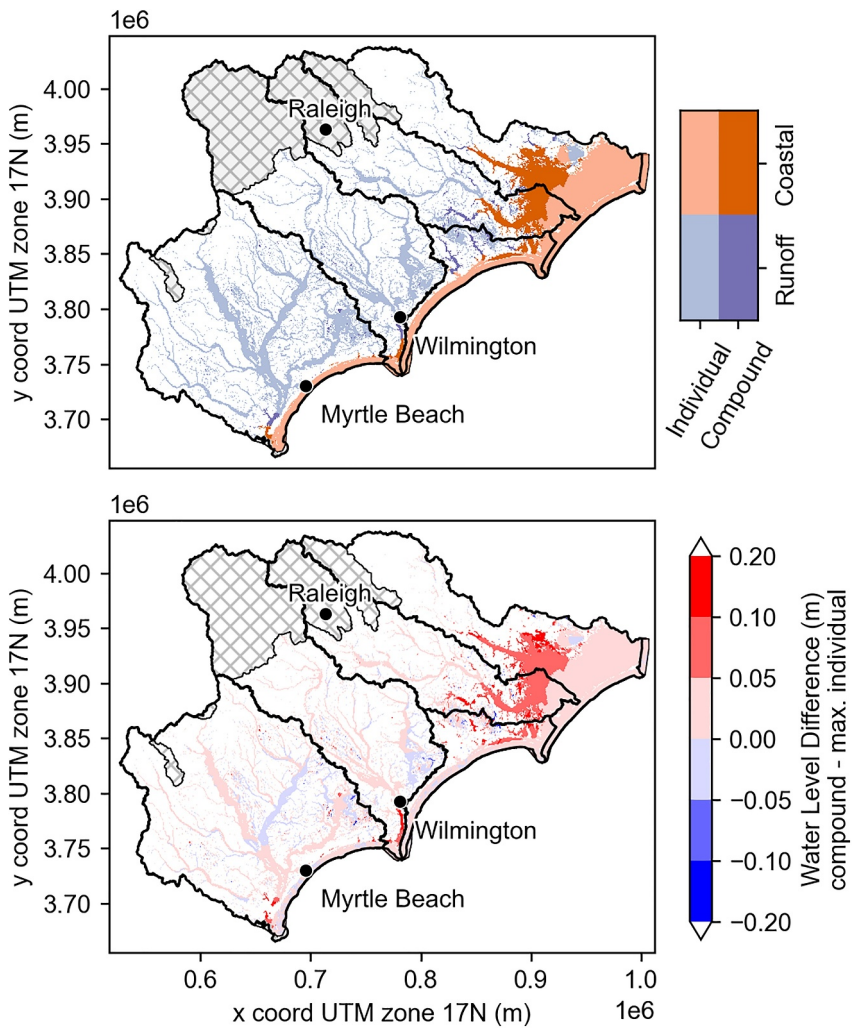

Figure 4. Attribution of peak flood inundation to runoff, coastal, and compound processes. The top panel (a) demonstrates which flood processes generated the greatest water levels across the model domain. Runoff-dominated areas are shown in purple and coastal-dominated areas are shown in orange. The darker shades of purple (runoff) and orange (coastal) indicate areas where the combination of the processes in the compound scenario exceed the maximum water level from either individual process by at least 0.05 m. The bottom panel (b) shows the difference in peak water levels between the compound scenario and the maximum depth from the individual processes. Red indicates that compound processes amplified total water levels.

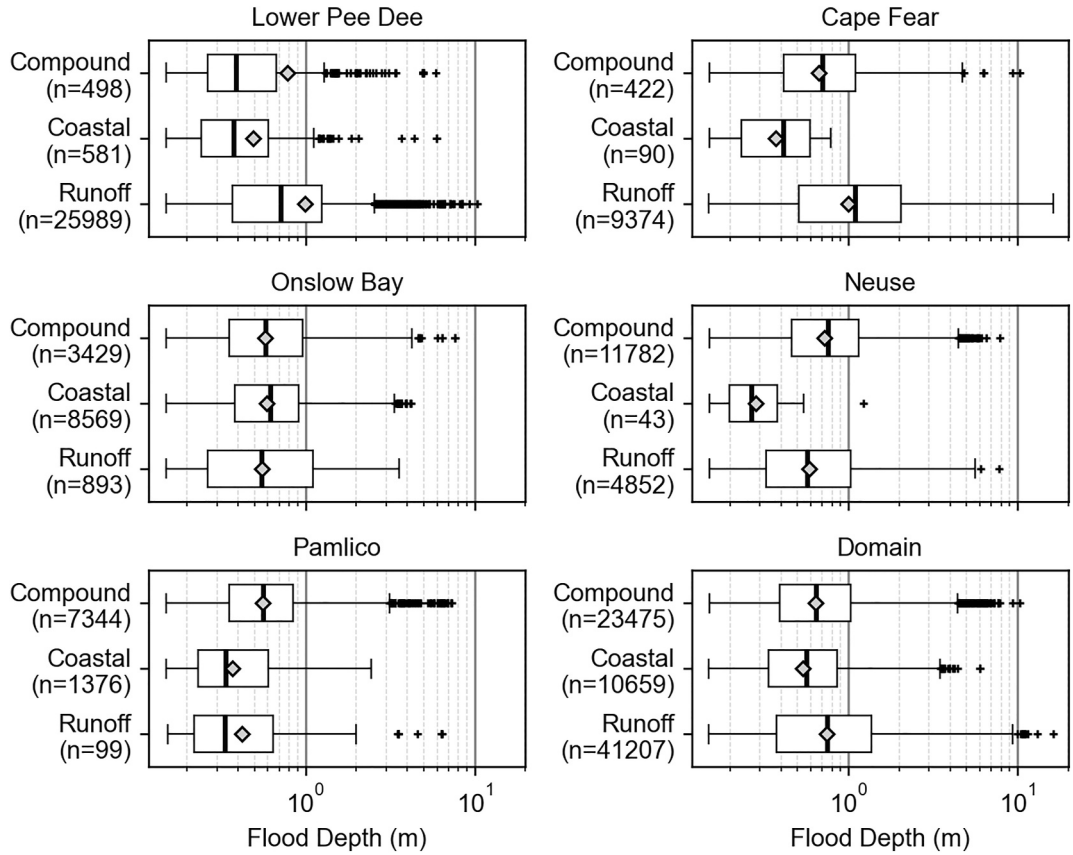

Figure 5. Boxplot of peak flood depths (>0.15 m) at buildings in each HUC6 basin and across the domain within the compound, coastal, and runoff peak flood extents. Water depth (m) is logged on the *x*-axis. The median is indicated by thick black line and the mean is noted by a gray diamond. The number of buildings (n) is listed below the scenario name.

Neuse, Onslow Bay and Pamlico, respectively. At buildings that were exposed to compound flooding, the maximum ground elevation was approximately 12, 13, 15, 37, and 69 m + NAVD88 in the Onslow Bay, Pamlico, Cape Fear, Neuse, and Lower Pee Dee watersheds, respectively (Figure 6b). Most buildings exposed to

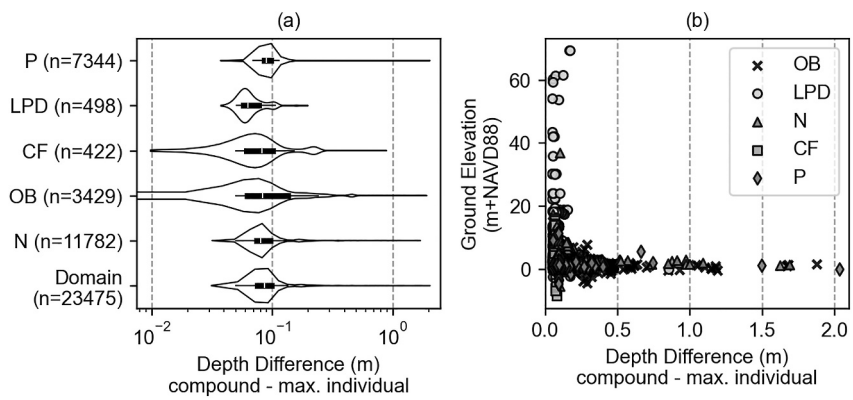

Figure 6. (a) Distribution of the change in peak water depths (m) at buildings (where the depth was greater than 0.15 m) due to compound processes grouped by HUC6 watershed and the entire domain. The *x*-axis is log scale. The width of each curve corresponds to the approximate frequency of the data in each region. The boxplot indicates the median and quartile ranges. The number of buildings (n) is listed below each group. (b) Elevation of the buildings that experienced inundation (>0.15 m) and the increase in the depth due to compound processes by HUC6 including the Onslow Bay (OB), Lower Pee Dee (LPD), Neuse (N), Cape Fear (CF), and Pamlico (P) watersheds.

10.1029/2023WR036727

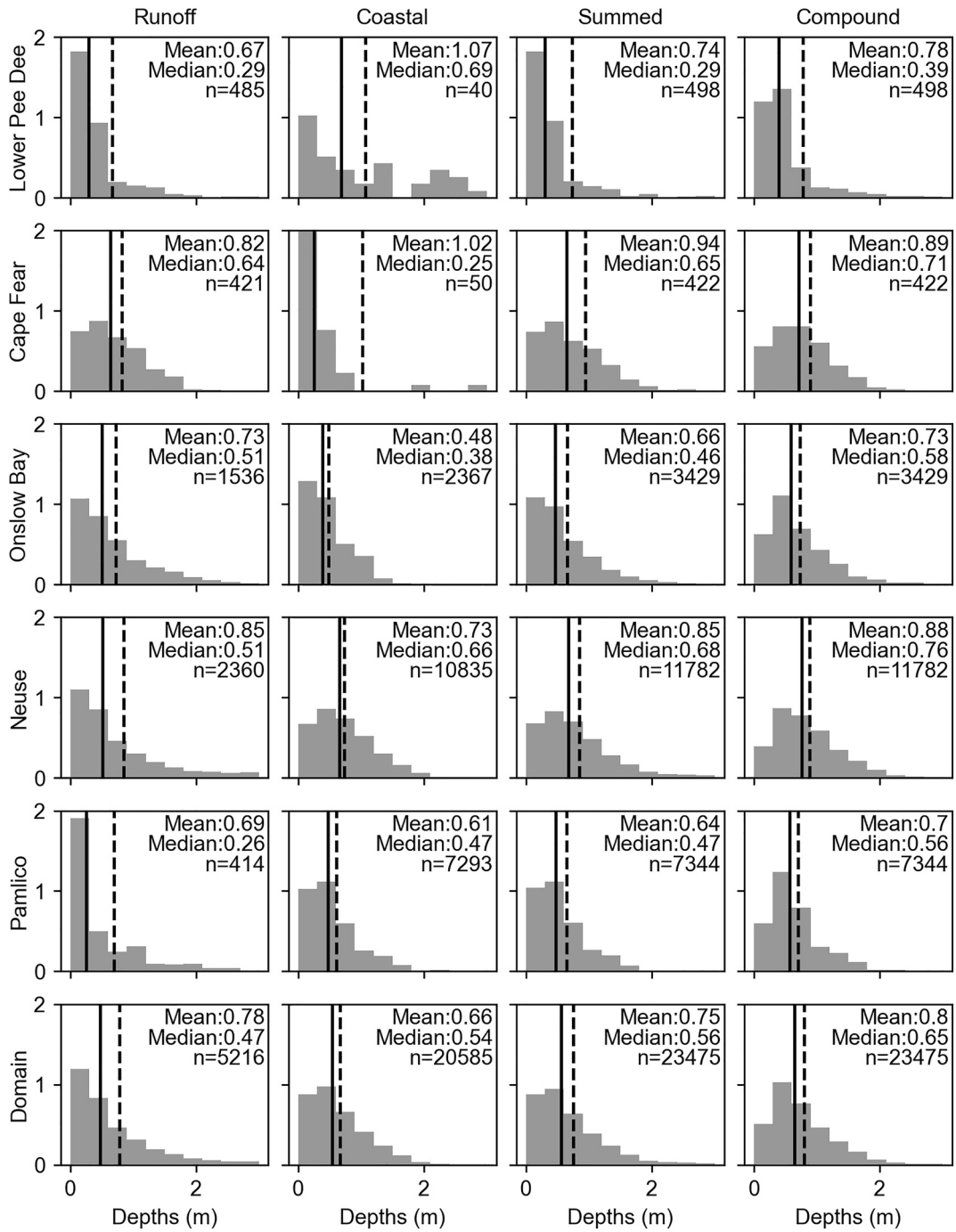

Figure 7. The distribution of flood depths (m) at buildings within the peak compound flood extent for the runoff, coastal, the linear addition of runoff and coastal depths (summed), and the compound processes (columns). The data is grouped by HUC6 watershed and for the entire domain (rows). The median is indicated by solid black line and the mean is a dashed black line. The mean, median, and number of buildings (n) are listed in each subplot.

compound flooding (23,167 or 98.7%) were located at lower elevations (mean and median were 2.0 and 1.6 m + NAVD88) with relatively few buildings (~40) located above 20 m + NAVD88.

For buildings located within the compound flood extent during Hurricane Florence, runoff processes generate depths that were on average 0.12 m greater than coastal processes (Figure 7). Compound processes exacerbate runoff depths by 0.02 m and coastal depths by 0.14 m on average. A simple linear summation of flood depths from

runoff and coastal processes leads to an underestimation of the mean flood depths by 0.05 m and median flood depths by 0.09 m (Figure 7).

5. Discussion

5.1. Model Performance

Across multiple performance metrics, our SFINCS model for the Carolinas shows skill when compared against reported water levels during Hurricane Florence and other storm events (see the Supporting Information S1 for model performance for Hurricane Matthew). When compared against HWM and gage measurements at 763 locations, the model peak water level error is spatially unbiased (0.11 m), but there is a large range in these errors (RMSE 0.92). Because HWMs are typically taken at vegetation, seed, mud, stain or debris lines on the ground or on buildings after flooding has receded, they are useful indicator of flooding beyond the channel banks or the mean high-water line at the coast. Here we used all HWMs that had a quality greater than 'Fair:±0.12 m'.

When compared against observed hydrographs at USGS gage stations (Figure S9 in Supporting Information S1), the model bias is negative, suggesting that the model underpredicts water levels on average across the entire 23-day simulation. This is especially true further inland in NC (except the Pamlico where we did not have data) where we assume rectangular channels of constant width and maximum depth, likely overestimating the cross-sectional area of flow and leading to low in-channel water levels when compared to observations during low or normal flow conditions (at the start and end of the simulation). Additionally, neglecting baseflow in the tributaries whose watersheds are fully contained within the model domain may also contribute to negative bias.

The performance metrics also suggest that river channel bathymetry is important for capturing inundation. As evidence of this, the model bias is smaller closer to the coast where improved bathymetry is available in national datasets. Higher Coefficient of Determination values in NC watersheds relative to those in SC indicate the model's predictive skill is better where channel bathymetry is specified to a finer degree. The model tends to overpredict water levels at gages in SC where channels were not highly resolved, suggesting that the collection and publication of bathymetric data is critical to the application of reduced-physics models at large scales for flood prediction and exposure analysis. Incorporating channels helps to route flow across watersheds, while neglecting to represent channels explicitly will displace flow into the floodplains, leading to an overestimate of peak inundation. To overcome the lack of high-resolution geospatial data, we assumed a constant depth of 2.0 m in the larger rivers of SC. This reduced the average peak error by 0.19 m indicating that even a simplified representation of channels in the terrain can improve modeled water levels (Table S3, Figure S5 in Supporting Information S1).

Reports of building damage have not been widely used to assess flood hazard model performance because data is typically only available aggregated to administrative units due to privacy concerns (Bates, 2023; Wing et al., 2020). Yet, flood hazard outputs are often used to estimate infrastructure exposure (Goulart et al., 2024; Schubert et al., 2024). Our model demonstrates that estimating exposure is complex. We find that the model correctly predicts flooding at building locations 83% of the time using a depth threshold of 1.5 m with a CSI of 0.67. These scores are similar to other studies that compare modeled flood extent to satellite images of flooding where well-validated models achieve values of 0.7–0.8 (Bates et al., 2021a; Courty et al., 2017; Sosa et al., 2020; Wing et al., 2017, 2021). While lower depth thresholds increase the number of false alarms the model predicts, the model is never able to predict flooding at all the locations that experienced damage, even when using a small depth threshold of 0.05 m (Bias: −0.20, POD of 0.67). This could be a result of fine-scale topographic features that are missing from the model terrain (e.g., presence/absence of barriers/conveyors of flow like culverts, roadways) or due to typical errors in the input data (e.g., precipitation, wind). Taking into consideration First Floor Elevation (FFE) data could yield different model results, possibly decreasing the number of false positives and true positives. However, FFE data outside the Federal Emergency Management Agency (FEMA) Special Flood Hazard Area (SFHA) are unknown, and policy holders may claim damage even when water does not exceed the first floor of the structure, due to, for example, impacts to electrical or other systems on the property.

When compared against depths at HWM locations and gage peaks, the model bias is 0.11 m with an RMSE of 0.92 m. Model error can be a useful indicator of depth thresholds to use for estimating a range of potential building exposure. In fact, larger depth thresholds (e.g., greater than 1.0 m) produced better performance metrics when evaluating building exposure. This could indicate that using smaller depth thresholds may lead to a conservative (high) estimate of the number of flooded buildings, even when the model shows skill compared against total water

levels. For example, using 0.15 m leads to 75,341 buildings exposed whereas using 1.0 m leads to 23,630 buildings exposed. The range in potential exposure also indicates the importance of considering structure elevation or differences in building vulnerability due to other types of adaptation (like flood proofing), for which there is limited data. This highlights the challenges and uncertainty in risk assessment using large scale models.

5.2. Flood Extent Attribution

Compound flooding accounts for 15.3% of the total area inundated from Hurricane Florence. Compound flooding is controlled in part by the spatial and temporal evolution of the hydrometeorological drivers (e.g., rainfall, wind). For example, in the Cape Fear, compound flooding was generated from rainfall at the inner core of a TC can contribute to compound flooding near the landfall location, especially as backwater effects from high coastal water levels (e.g., storm tide) prevent drainage in the watershed systems impacting water levels by 0.10–0.20 m. Gori, Lin, and Xi (2020) and Bao et al. (2024) describe similar dynamics in the lower Cape Fear watershed, but with a larger model domain, we are able to demonstrate how the drivers of flood processes vary across multiple watersheds.

The peak compound flood extent was greatest in watersheds located east of the landfall location. The total area of the peak compound extent in the Pamlico and Neuse (1,620 sq. km.) was over five times larger than in the Cape Fear and Lower Pee Dee combined (288 sq. km.). In the Lower Pee Dee and Cape Fear, runoff process contributed to 96% of the peak flood extent with compound processes only contributed 3% (primarily at the lower end of the estuaries). In the Neuse and Onslow Bay watersheds, compound flooding contributed to 29% and 31% of the peak flood extent, respectively as surge interacted with peak streamflow generated by highly concentrated rainfall. Runoff processes were the largest contributor of peak flood extent in all watersheds except for the Pamlico, where compound processes were the largest contributor at 46%. The Pamlico—farthest from the storm's landfall—experienced peak surge levels due to high winds at the edge of the storm (similar to the Neuse), but less rainfall compared to the other watersheds. It is possible that the lower amount of rainfall over the Pamlico that occurred in larger, evenly spread swaths that enable storm surge to propagate far upstream to interact with local rainfall-runoff compared to in the Neuse where higher stream flows from intense rainfall prevented the inland propagation of storm surge.

Across the entire domain, we generally found that areas that experienced the greatest increase in water level due to the combination of flood processes were primarily below 20 m + NAVD88, but in some cases, process interactions influence water levels far upriver (e.g., in the Neuse where channel data was best). Topography also impacts how likely runoff and coastal processes are to interact. For example, storm surge is funneled into the Cape Fear and Black River at Wilmington due to topographic ridges separating the floodplains (e.g., 10 m) as well as high bounding elevations inland of 20 m and at the coast of 15 m. The geography of the Lower Pee Dee estuary is very similar to the Neuse (e.g., shape and orientation, confluence of rivers) but elevations are generally lower which is characteristic of the lowlands. At the outlet of the Lower Pee Dee watershed, the confluence of the Great Pee Dee and Waccamaw rivers includes much more interconnected floodplains which can facilitate widespread exchange of both coastal and runoff processes across a wider area than the Neuse (~28 km from coastal high of 8 m to inland 15 m ridge). Compared to these estuaries, the Neuse and Pamlico estuaries have more defined riverbanks which can aid in the channelization of storm surge inland which occurred during Hurricane Florence.

The size and shape of the watershed will impact how streamflow is generated. For example, the time of concentration of the larger rivers in the Carolinas is on the order of multiple days (and up to a week) which will influence the interaction of peak streamflow and surge. For Florence, most of the estuaries of these major rivers experienced a double peak in the hydrograph where storm surge had largely receded by the time peak streamflow arrived. This resulted in amplified water levels and extended durations of flooding. We also note that capturing the residence time of coastal processes in the estuaries is important for how far inland compound flooding can occur (e.g., post storm onshore/offshore winds). The smaller tributaries within the larger HUC6 watersheds (e.g., Trent River (Neuse), Northeast Cape Fear River (Cape Fear), and White Oak River (Onslow Bay) had a more direct interaction between storm surge and peak streamflow due to their shorter times of concentration.

Our findings have implications for our understanding of compound flooding in other locations around the United States and globally. We expect that in areas with higher topographic relief or more incised channels, the inland propagation of compound flooding may be greater, but the extent will be largely controlled by the riverbanks.

Conversely, in lower-gradient areas, like the U.S. Gulf Coast, the extent of compound flooding may be expansive though depths potentially shallower as flood water is able to spread across the shallow floodplains.

5.3. Building Exposure

From previous studies, it is evident that compound processes occur in the main river channels and large water bodies (Bao et al., 2022; Bilskie et al., 2021; Gori, Lin, & Smith, 2020; Maymandi et al., 2022; Zhang et al., 2020), but our study investigates how these physical interactions might alter building exposure located further away from waterbodies. We estimate that more than 75,341 buildings were exposed to inundation depths > 0.15 m with compound processes accounting for 31% of exposed buildings. We find that the interaction between runoff and coastal processes at exposed buildings is nonlinear and summing the depths generated by the individual processes is not a substitution for simulating their interactions (e.g., Bao et al., 2024; Bilskie & Hagen, 2018). In fact, our analysis suggests that during Hurricane Florence compound processes acted as a threat multiplier and that simply adding depths from runoff and coastal processes would underestimate total damages.

Our results indicate that the relative contribution of the flood processes to the peak flood extent is not a proxy for exposure, but rather, exposure is a function of both where development has historically occurred and the characteristics of the storm. Runoff process contributed the most to both peak flood extent and building exposure. However, the role of the other processes was also relevant to estimating building exposure. For example, compound processes contributed to 15% of the total flood extent but they contributed 31% of building exposure. Similarly, while coastal processes didn't contribute to the overall inundation (~6%) they contributed 14% of the total building exposure with the lowest mean depths of 0.66 m. Of the buildings exposed, 36% were in the Lower Pee Dee. Despite its proximity to the landfall location and the concentration of population in the Cape Fear Basin, we estimate that buildings in the Cape Fear basin contributed only accounted for 13% of the total number exposed buildings. While the extent of compounding of water levels was greatest in the Pamlico basin, the buildings exposed were only 12% of the total exposed buildings. In general, buildings below 20 m + NAVD88 were the most exposed to compound flooding but runoff processes from Hurricane Florence generated the greatest amount of exposure across the Carolinas.

5.4. Limitations and Challenges

The model performance results suggest that representing channel bathymetry in the model is important. While we did not do a detailed sensitivity analysis of the influence of different channel assumptions, we did test the model without any channels represented and found that it increases the average peak error by 0.19 m. The advantage of reduced-complexity models is that they can efficiently simulate multiple flood processes at large scales, leveraging large datasets, but the accurate representation of channels and their influence on flood routing is critical to achieving improved model performance (Cooper, 2002; Dey et al., 2019; Harrison et al., 2022; Leuven et al., 2018; Slater, 2016; Yankovsky et al., 2012). Despite the evidence that channels are important, there is still a lack of However, there remains very limited readily accessible information on data on river bathymetry or tools for incorporating them into models (Neal et al., 2021) which makes modeling flooding at large spatial scales a challenge. This work provides further evidence of the need for improved bathymetric data given the scale of infrastructure exposed to TC flooding and the complexities between the interactions in coastal and runoff processes that primarily occur in channels but determine channel-floodplain interactions and thus inundation extent.

In addition to river channel bathymetry, there are other several other potential sources of uncertainty. First, we did not explicitly account for streamflow obstructions, such as small weirs/dams or bridge piers, which can alter the propagation of streamflow and possibly slow down channel flow which could impact the shape of the hydrograph (Bates, 2021). There are ongoing efforts to create databases of infrastructure (Nienhuis et al., 2022) and corrected DEMs that can be incorporated into models (Schumann & Bates, 2018; Woodrow et al., 2016). Second, we did not account for subsurface infrastructure (e.g., storm sewers), but we would expect their influence on the extent of pluvial flooding to be small as they were likely at capacity given the size of this event relative to their design. Third, there is some uncertainty in the total volume of rainfall-runoff the model generates due to uncertainty in land cover, imperviousness, and soil quality, but other infiltration schemes (such as Green and Ampt Loss Method) can harness additional information for improved runoff estimation. Finally, the quality of the input data (e.g., meteorological inputs) can contribute to model errors when hindcasting hydrodynamic processes resulting from TCs (Rahman et al., 2022; Ratcliff, 2022). For example, spatiotemporal variations in rainfall will impact the

timing and volume of runoff (Quintero et al., 2016). Using an ensemble of data can help address these issues, providing an estimate of uncertainty (Grimley et al., 2020).

6. Conclusions

Flood exposure from TCs can extend far beyond coastal areas as extreme rainfall can generate significant pluvial and fluvial flooding that can exacerbate flooding in coastal communities and further inland (Gori, Lin, & Xi, 2020; Pricope et al., 2022; Sebastian et al., 2021). In this study, we complete an in-depth validation of the reduced-complexity hydrodynamic model (SFINCS) one-way coupled to an ocean circulation model (ADCIRC). We chose SFINCS because it represents processes important for simulating TC flooding (e.g., wind, sea level, rainfall, streamflow) and is fast, scalable, and readily applied using open-source tools. We hindcast runoff and coastal processes from Hurricane Florence to predict water levels across five HUC6 watersheds in the Carolinas and perform a detailed evaluation of the model performance, comparing against observed water levels (89 water level gages, 763 HWM locations) and property-level records of insured damage (22,812 buildings). Our study provides new insights into model performance in inland areas (e.g., >20 m + NAVD88). The model shows skill in simulating the peak water levels with a bias of 0.11 m and RMSE of 0.92 m, and correctly predicts flood exposure at 83% of structures using a depth threshold of 1.0 m.

Overall, runoff processes were the primary driver of peak flood extent and building exposure from Hurricane Florence because the storm stalled over the Carolinas for several days, generating significant rainfall totals. In total, compound flooding accounted for only 15% of the area inundated, yet one third (31%) of building exposure to inundation greater than 0.15 m was attributed to compound processes. We demonstrate that the interactions between coastal and runoff processes are nonlinear, leading to greater water levels at exposed structures than either of runoff or coastal processes. During Hurricane Florence, compound flooding primarily occurred in watersheds far away from the landfall location. However, it is important to note that this area can shift depending on the initial conditions of the system (e.g., mean sea level, streamflow) and the spatial variations in the meteorology (wind, rainfall) associated with a given TC. Future work should consider multiple storms and geographic systems to further understand what controls compound flooding.

Data Availability Statement

The SFINCS modeled maximum water levels and depths for Hurricane Florence can be downloaded from DesignSafe https://doi.org/10.17603/ds2-m3ag-2d15 (Grimley et al., 2025). The DEM used to define elevations in the SFINCS model can be obtained from DesignSafe https://doi.org/10.17603/ds2-mzc8-s589 (Grimley & Sebastian, 2025). Multi-Radar/Multi-Sensor System (MRMS) radar rainfall data can be downloaded from the Iowa Environmental Mesonet (IEM) archive (IEM, 2024). OWI wind data for Hurricane Florence is proprietary data from OceanWeather Inc. USGS HWMs can be downloaded from the USGS Flood Event Viewer (USGS, 2024a). HWMs taken by North Carolina Geologic Survey were obtained from North Carolina Emergency Management; inquiries regarding this data may be sent to frishelp@ncdps.gov. Water level gage data can be downloaded directly from USGS's National Water Dashboard (USGS, 2024c) and NOAA (NOAA, 2024a). USGS Coastal National Elevation Dataset (CoNED) and National Elevation Dataset (NED) can be downloaded from the USGS National Map (USGS, 2024b). LiDAR-derived DEMs for NC can be downloaded directly from NC OneMap (NCEM, 2024b) and HEC-RAS models can be downloaded from the NC Flood Risk Information System (FRIS) (NCEM, 2024a). NOAA's Vertical Datum Transformation v4.3 tool was used to convert all elevation data to NAVD88 (NOAA, 2024b). NLCD land cover data can be downloaded from Multi-Resolution Land Characteristics (MRLC) Consortium (MRLC, 2022). We used Gridded National Soil Survey Geographic Database (gNATSGO) which can be downloaded from USDA-NRCS Soil & Plant Science Division (SPSD) composite database (Soil Survey Staff, 2022). Levee data can be downloaded directly from the National Levee Database (USACE, 2024a). As part of a study of Hurricane Florence commissioned by the NC Legislature (NC Policy Collaboratory, 2021), we obtained address records of Federal Insurance and Mitigation Administration (FIMA) National Flood Insurance Program (NFIP) policies and claims data for 77 counties in NC from FEMA Region IV. The property level version of insurance policies and claims data used in this analysis is confidential, although inquiries regarding availability may be sent to OpenFEMA@fema.dhs.gov. NFIP claims and policy addresses were geocoded and joined to a dataset of building footprints obtained from NC OneMap (NCEM, 2024b). SC buildings data can be downloaded directly from the USACE's National Structure Inventory

(USACE, 2024b). We used the SFINCS version 2.0.2 Blockhaus which can be downloaded here https://zenodo.org/record/8038565 (van Ormondt et al., 2023). The SFINCS model was constructed using the python package hydroMT-sfincs v.0.2.1 which can be downloaded here https://zenodo.org/records/6244556 (Eilander et al., 2022). Hurricane Matthew ADCIRC storm surge data can be downloaded from DesignSafe (Asher, 2019).

Acknowledgments
We thank K. Fitzmaurice at the Institute for Risk Management and Insurance Innovation (IRMII) at UNC Chapel Hill for helping to geocode the property-level data. We would also like to acknowledge K. Nederhoff, M. van Ormondt and R. de Goede at Deltares for fruitful discussion and software support and four anonymous reviewers who provided constructive feedback to improve the manuscript. This research was supported by the North Carolina General Assembly and the North Carolina Policy Collaboratory through Session Law 2019-224. L.E.G., A.S., and R.L. were supported by the National Science Foundation (GCR-2021086) as a part of the Dynamics of Extreme Events, People, and Places (DEEPP) project at the University of North Carolina at Chapel Hill. L.E.G. was also supported by a graduate research fellowship with the North Carolina Water Resources Research Institute (WRRI) and North Carolina Sea Grant. The authors are grateful to the North Carolina Department of Emergency Management and FEMA Region IV for access to data. The authors declare no conflicts of interest relevant to this study.

References

Asher, T. (2019). Hurricane Matthew storm surge and wave simulations [Dataset]. *DesignSafe*. https://doi.org/10.17603/ds2-ne6j-s897

Bakhtyar, R., Maitaria, K., Velissariou, P., Trimble, B., Mashriqui, H., Moghimi, S., et al. (2020). A New 1D/2D coupled modeling approach for a riverine-estuarine system under storm events: Application to Delaware river basin. *Journal of Geophysical Research: Oceans*, *125*(9). https://doi.org/10.1029/2019JC015822

Bao, D., Xue, Z. G., & Warner, J. C. (2024). Quantifying compound and nonlinear effects of hurricane-induced flooding using a dynamically coupled hydrological-ocean model. *Water Resources Research*, *60*(7). https://doi.org/10.1029/2023WR036455

Bao, D., Xue, Z. G., Warner, J. C., Moulton, M., Yin, D., Hegermiller, C. A., et al. (2022). A numerical investigation of hurricane florence-induced compound flooding in the Cape fear estuary using a dynamically coupled hydrological-ocean model. *Journal of Advances in Modeling Earth Systems*, *14*(11). https://doi.org/10.1029/2022MS003131

Bates, P. D. (2021). Flood inundation prediction. *Annual Review of Fluid Mechanics*, *54*(1), 287–315. https://doi.org/10.1146/annurev-fluid-030121-113138

Bates, P. D. (2023). Fundamental limits to flood inundation modelling. *Nature Water*, *1*(7), 566–567. https://doi.org/10.1038/s44221-023-00106-4

Bates, P. D., Quinn, N., Sampson, C., Smith, A., Wing, O., Sosa, J., et al. (2021a). Combined modeling of US fluvial, pluvial, and coastal flood hazard under current and future climates. *Water Resources Research*, *57*(2), 1–29. https://doi.org/10.1029/2020WR028673

Bates, P. D., Quinn, N., Sampson, C., Smith, A., Wing, O., Sosa, J., et al. (2021b). Combined modeling of US fluvial, pluvial, and coastal flood hazard under current and future climates. *Water Resources Research*, *57*(2), 1–29. https://doi.org/10.1029/2020WR028673

Bertoncelj, V., Leijnse, T., Roelvink, F., Pearson, S., Bricker, J., Tissier, M., & Van Dongeren, A. (2021). Efficient and accurate modeling of wave-driven flooding on coral reef-lined coasts: Case study of Majuro Atoll, Republic of the Marshall Islands. In *EGU general Assembly*. https://doi.org/10.5194/egusphere-egu21-5418

Bilskie, M. V., & Hagen, S. C. (2018). Defining flood zone transitions in low-gradient coastal regions. *Geophysical Research Letters*, *45*(6), 2761–2770. https://doi.org/10.1002/2018GL077524

Bilskie, M. V., Zhao, H., Resio, D., Atkinson, J., Cobell, Z., & Hagen, S. C. (2021). Enhancing flood hazard assessments in coastal Louisiana through coupled hydrologic and surge processes. *Frontiers in Water*, *3*. https://doi.org/10.3389/frwa.2021.609231

Casulli, V. (2009). A high-resolution wetting and drying algorithm for free-surface hydrodynamics. *International Journal for Numerical Methods in Fluids*, *60*(4), 391–408. https://doi.org/10.1002/fld.1896

Chow, V. T., Maidment, D. R., & Mays, L. W. (1998). *In Applied hydrology. B. J. Clark & J. Morriss, Eds*. McGraw-Hill Book Company. Retrieved from http://ponce.sdsu.edu/Applied_Hydrology_Chow_1988.pdf

Colle, B. A., Buonaiuto, F., Bowman, M. J., Wilson, R. E., Flood, R., Hunter, R., et al. (2008). New York City's vulnerability to coastal flooding. *Bulletin of the American Meteorological Society*, *89*(6), 829–842. https://doi.org/10.1175/2007BAMS2401.1

Cooper, J. A. G. (2002). The role of extreme floods in estuary-coastal behaviour: Contrasts between river- and tide-dominated microtidal estuaries. *Sedimentary Geology*, *150*(1–2), 123–137. https://doi.org/10.1016/S0037-0738(01)00271-8

Courty, L. G., Pedrozo-Acuña, A., & Bates, P. D. (2017). Itzï (version 17.1): An open-source, distributed GIS model for dynamic flood simulation. *Geoscientific Model Development*, *10*(4), 1835–1847. https://doi.org/10.5194/gmd-10-1835-2017

Dey, S., Saksena, S., & Merwade, V. (2019). Assessing the effect of different bathymetric models on hydraulic simulation of rivers in data sparse regions. *Journal of Hydrology*, *575*(July 2018), 838–851. https://doi.org/10.1016/j.jhydrol.2019.05.085

Dietrich, J. C., Westerink, J. J., Kennedy, A. B., Smith, J. M., Jensen, R. E., Zijlema, M., et al. (2011). Hurricane Gustav (2008) waves and storm surge: Hindcast, synoptic analysis, and validation in Southern Louisiana. *Monthly Weather Review*, *139*(8), 2488–2522. https://doi.org/10.1175/2011MWR3611.1

Eilander, D., Boisgontier, H., Bouaziz, L. J. E., Buitink, J., Couasnon, A., Dalmijn, B., et al. (2023). HydroMT: Automated and reproducible model building and analysis. *Journal of Open Source Software*, *8*(83), 4897. https://doi.org/10.21105/joss.04897

Eilander, D., Couasnon, A., Leijnse, T., Ikeuchi, H., Yamazaki, D., Muis, S., et al. (2023). A globally applicable framework for compound flood hazard modeling. *Natural Hazards and Earth System Sciences*, *23*(2), 823–846. https://doi.org/10.5194/nhess-23-823-2023

Eilander, D., Couasnon, A., Sperna Weiland, F. C., Ligtvoet, W., Bouwman, A., Winsemius, H. C., & Ward, P. J. (2023). Modeling compound flood risk and risk reduction using a globally applicable framework: A pilot in the Sofala province of Mozambique. *Natural Hazards and Earth System Sciences*, *23*(6), 2251–2272. https://doi.org/10.5194/nhess-23-2251-2023

Eilander, D., Leijnse, T., & Winsemius, H. C. (2022). hydroMT-sfincs (v0.2.1). Zenodo. https://doi.org/10.5281/zenodo.6244556

EPA. (2015). Storm water management model reference manual volume I. Retrieved from https://cfpub.epa.gov/si/si_public_record_report.cfm?Lab=NRMRL&dirEntryId=309346

Garratt, J. R. (1977). Review of drag coefficients over oceans and continents. *Monthly Weather Review*, *105*(7), 915–929. https://doi.org/10.1175/1520-0493(1977)105<0915:RODCOO>2.0.CO;2

Gori, A., Lin, N., & Smith, J. (2020). Assessing compound flooding from landfalling tropical cyclones on the North Carolina Coast. *Water Resources Research*, *56*(4). https://doi.org/10.1029/2019WR026788

Gori, A., Lin, N., & Xi, D. (2020). Tropical cyclone compound flood hazard assessment: From investigating drivers to quantifying extreme water levels. *Earth's Future*, *8*(12). https://doi.org/10.1029/2020EF001660

Gori, A., Lin, N., Xi, D., & Emanuel, K. (2022). Tropical cyclone climatology change greatly exacerbates US extreme rainfall–surge hazard. *Nature Climate Change*, *12*(2), 171–178. https://doi.org/10.1038/s41558-021-01272-7

Goulart, H. M. D., Benito Lazaro, I., Van Garderen, L., Van Der Wiel, K., Le Bars, D., Koks, E., & Van Den Hurk, B. (2024). Compound flood impacts from Hurricane Sandy on New York City in climate-driven storylines. *Natural Hazards and Earth System Sciences*, *24*(1), 29–45. https://doi.org/10.5194/nhess-24-29-2024

Grimley, L. E., Quintero, F., & Krajewski, W. F. (2020). Streamflow predictions in a small urban–rural watershed: The effects of radar rainfall resolution and urban rainfall–runoff dynamics. *Atmosphere*, *11*(8), 774. https://doi.org/10.3390/atmos11080774

Grimley, L. E., & Sebastian, A. (2025). Topobathymetric digital elevation models (DEM) for flood modeling in the Carolinas (version 1) [dataset]. *DesignSafe-CI*. https://doi.org/10.17603/ds2-mzc8-s589

Grimley, L. E., Sebastian, A., Leijnse, T., Eilander, D., Ratcliff, J., & Luettich, R. (2025). Hydrodynamic modeling of runoff, coastal, and compound flood processes during Hurricane Florence across the Carolinas [dataset]. *DesignSafe-CI*. https://doi.org/10.17603/ds2-m3ag-2d15

Grinsted, A., Ditlevsen, P., & Christensen, J. H. (2019). Normalized US hurricane damage estimates using area of total destruction, 1900−2018. *Proceedings of the National Academy of Sciences*, *116*(48), 23942–23946. https://doi.org/10.1073/pnas.1912277116

Hall, T. M., & Kossin, J. P. (2019). Hurricane stalling along the North American coast and implications for rainfall. *Npj Climate and Atmospheric Science*, *2*(1), 17. https://doi.org/10.1038/s41612-019-0074-8

Hallegatte, S., Green, C., Nicholls, R. J., & Corfee-Morlot, J. (2013). Future flood losses in major coastal cities. *Nature Climate Change*, *3*(9), 802–806. https://doi.org/10.1038/nclimate1979

Harrison, L. M., Coulthard, T. J., Robins, P. E., & Lewis, M. J. (2022). Sensitivity of estuaries to compound flooding. *Estuaries and Coasts*, *45*(5), 1250–1269. https://doi.org/10.1007/s12237-021-00996-1

Hoeppe, P. (2016). Trends in weather related disasters – Consequences for insurers and society. *Weather and Climate Extremes*, *11*, 70–79. https://doi.org/10.1016/j.wace.2015.10.002

IEM. (2024). *Multi-radar/multi-sensor system (MRMS) QPE*. Iowa Environmental Mesonet Archive. Retrieved from https://mesonet.agron.iastate.edu/

Jackson, E. K., Roberts, W., Nelsen, B., Williams, G. P., Nelson, E. J., & Ames, D. P. (2019). Introductory overview: Error metrics for hydrologic modelling – a review of common practices and an open source library to facilitate use and adoption. *Environmental Modelling & Software*, *119*(May), 32–48. https://doi.org/10.1016/j.envsoft.2019.05.001

Klotzbach, P. J., Bowen, S. G., Pielke, R., & Bell, M. (2018). Continental U.S. Hurricane landfall frequency and associated damage: Observations and future risks. *Bulletin of the American Meteorological Society*, *99*(7), 1359–1376. https://doi.org/10.1175/BAMS-D-17-0184.1

Klotzbach, P. J., Wood, K. M., Schreck, C. J., Bowen, S. G., Patricola, C. M., & Bell, M. M. (2022). Trends in global tropical cyclone Activity: 1990–2021. *Geophysical Research Letters*, *49*(6). https://doi.org/10.1029/2021GL095774

Krause, P., Boyle, D. P., & Bäse, F. (2005). Comparison of different efficiency criteria for hydrological model assessment. *Advances in Geosciences*, *5*, 89–97. https://doi.org/10.5194/adgeo-5-89-2005

Kunkel, K. E., & Champion, S. M. (2019). An assessment of rainfall from hurricanes Harvey and florence relative to other extremely wet storms in the United States. *Geophysical Research Letters*, *46*(22), 13500–13506. https://doi.org/10.1029/2019GL085034

Lai, Y., Li, J., Gu, X., Liu, C., & Chen, Y. D. (2021). Global compound floods from precipitation and storm surge: Hazards and the roles of cyclones. *Journal of Climate*, *34*(20), 1–55. https://doi.org/10.1175/JCLI-D-21-0050.1

Leijnse, T., Nederhoff, K., Van Dongeren, A., McCall, R., & Van Ormondt, M. (2020). Improving computational efficiency of compound flooding simulations: The SFINCS model with subgrid features. In Agufm. *Online: Agu*. Retrieved from https://agu2020fallmeeting-agu.ipostersessions.com/Default.aspx?s=9C-05-18-CF-F1-2B-17-F0-7A-21-93-E6-13-AE-F3-24

Leijnse, T., Van Ormondt, M., Nederhoff, K., & Van Dongeren, A. (2021). Modeling compound flooding in coastal systems using a computationally efficient reduced-physics solver: Including fluvial, pluvial, tidal, wind- and wave-driven processes. *Coastal Engineering*, *163*(December 2019), 103796. https://doi.org/10.1016/j.coastaleng.2020.103796

Leuven, J. R. F. W., Van Maanen, B., Lexmond, B. R., Van Der Hoek, B. V., Spruijt, M. J., & Kleinhans, M. G. (2018). Dimensions of fluvial-tidal meanders: Are they disproportionally large? *Geology*, *46*(10), 923–926. https://doi.org/10.1130/G45144.1

Liu, Q., Xu, H., & Wang, J. (2022). Assessing tropical cyclone compound flood risk using hydrodynamic modelling: A case study in Haikou city, China. *Natural Hazards and Earth System Sciences*, *22*(2), 665–675. https://doi.org/10.5194/nhess-22-665-2022

Liu, Z., Merwade, V., & Jafarzadegan, K. (2019). Investigating the role of model structure and surface roughness in generating flood inundation extents using one- and two-dimensional hydraulic models. *Journal of Flood Risk Management*, *12*(1). https://doi.org/10.1111/jfr3.12347

Loveland, M., Kiaghadi, A., Dawson, C. N., Rifai, H. S., Misra, S., Mosser, H., & Parola, A. (2021). Developing a modeling framework to simulate compound flooding: When storm surge interacts with riverine flow. *Frontiers in Climate*, *2*(February). https://doi.org/10.3389/fclim.2020.609610

Maymandi, N., Hummel, M. A., & Zhang, Y. (2022). Compound coastal, fluvial, and pluvial flooding during historical hurricane events in the Sabine–Neches Estuary, Texas. *Water Resources Research*, *58*(12). https://doi.org/10.1029/2022WR033144

Meiler, S., Vogt, T., Bloemendaal, N., Ciullo, A., Lee, C.-Y., Camargo, S. J., et al. (2022). Intercomparison of regional loss estimates from global synthetic tropical cyclone models. *Nature Communications*, *13*(1), 6156. https://doi.org/10.1038/s41467-022-33918-1

Merkens, J.-L., Reimann, L., Hinkel, J., & Vafeidis, A. T. (2016). Gridded population projections for the coastal zone under the Shared Socioeconomic Pathways. *Global and Planetary Change*, *145*, 57–66. https://doi.org/10.1016/j.gloplacha.2016.08.009

MRLC. (2022). Multi-resolution land characteristics consortium. Retrieved from https://www.mrlc.gov/

NCEI. (2023). NOAA national centers for environmental information (NCEI) U.S. Billion-dollar weather and. *Climate Disasters*. https://doi.org/10.25921/stkw-7w73

NCEM. (2024a). North Carolina flood risk information system (FRIS). Retrieved from https://fris.nc.gov/

NCEM. (2024b). North Carolina one Map. Retrieved from https://www.nconemap.gov/

NC Policy Collaboratory. (2021). Collaboratory flood resiliency study. Retrieved from https://collaboratory.unc.edu/wp-content/uploads/sites/476/2021/06/flood-resiliency-report.pdf

Neal, J., Dunne, T., Sampson, C., Smith, A., & Bates, P. D. (2018). Optimisation of the two-dimensional hydraulic model LISFOOD-FP for CPU architecture. *Environmental Modelling & Software*, *107*(May), 148–157. https://doi.org/10.1016/j.envsoft.2018.05.011

Neal, J., Hawker, L., Savage, J., Durand, M., Bates, P., & Sampson, C. (2021). Estimating River channel bathymetry in large scale flood inundation models. *Water Resources Research*, *57*(5), 1–22. https://doi.org/10.1029/2020WR028301

Neal, J., Schumann, G., & Bates, P. D. (2012). A subgrid channel model for simulating river hydraulics and floodplain inundation over large and data sparse areas. *Water Resources Research*, *48*(11), 1–16. https://doi.org/10.1029/2012WR012514

Nederhoff, K., Leijnse, T., Parker, K., Thomas, J., O'Neill, A., Van Ormondt, M., et al. (2023). Tropical or extratropical cyclones: What drives the compound flood hazard, impact, and risk for the United States Southeast Atlantic coast? *EarthArXiv*. https://doi.org/10.31223/X56H26

Nederhoff, K., Leijnse, T. W. B., Parker, K., Thomas, J., O'Neill, A., Van Ormondt, M., et al. (2024). Tropical or extratropical cyclones: What drives the compound flood hazard, impact, and risk for the United States Southeast Atlantic coast? *Natural Hazards*, *120*(9), 8779–8825. https://doi.org/10.1007/s11069-024-06552-x

Nienhuis, J. H., Cox, J. R., O'Dell, J., Edmonds, D. A., & Scussolini, P. (2022). A global open-source database of flood-protection levees on river deltas (openDELvE). *Natural Hazards and Earth System Sciences*, *22*(12), 4087–4101. https://doi.org/10.5194/nhess-22-4087-2022

NOAA. (2024a). NOAA tides and currents. Retrieved from https://tidesandcurrents.noaa.gov/

NOAA. (2024b). NOAA's vertical Datum transformation (version 4.7). *Software*. Retrieved from https://vdatum.noaa.gov/

NOAA, & NHC. (2023). Tropical cyclone climatology. Retrieved from https://www.nhc.noaa.gov/climo/
Pörtner, H.-O., Roberts, D. C., Poloczanska, E. S., Mintenbeck, K., Tignor, M., Alegría, A., et al. (2023). IPCC, 2022: Summary for policymakers. In *Climate change 2022 – impacts, adaptation and vulnerability* (pp. 3–34). Cambridge University Press. https://doi.org/10.1017/9781009325844.001
Pricope, N. G., Hidalgo, C., Pippin, J. S., & Evans, J. M. (2022). Shifting landscapes of risk: Quantifying pluvial flood vulnerability beyond the regulated floodplain. *Journal of Environmental Management*, *304*(December 2021), 114221. https://doi.org/10.1016/j.jenvman.2021.114221
Quintero, F., Krajewski, W. F., Mantilla, R., Small, S., & Seo, B.-C. (2016). A spatial–Dynamical framework for evaluation of satellite rainfall products for flood prediction. *Journal of Hydrometeorology*, *17*(8), 2137–2154. https://doi.org/10.1175/JHM-D-15-0195.1
Rahman, M. A., Zhang, Y., Lu, L., Moghimi, S., Hu, K., & Abdolali, A. (2022). Relative accuracy of HWRF reanalysis and a parametric wind model during the landfall of Hurricane Florence and the impacts on storm surge simulations. *Natural Hazards*, *116*(1), 904. https://doi.org/10.1007/s11069-022-05702-3
Ratcliff, J. (2022). Analysis of wind and storm surge of hurricane florence. https://doi.org/10.17615/zrvv-mq88
Ray, T., Stepinski, E., Sebastian, A., & Bedient, P. B. (2011). Dynamic modeling of storm surge and inland flooding in a Texas coastal floodplain. *Journal of Hydraulic Engineering*, *137*(10), 1103–1110. https://doi.org/10.1061/(asce)hy.1943-7900.0000398
Röbke, B. R., Leijnse, T., Winter, G., Van Ormondt, M., Van Nieuwkoop, J., & De Graaff, R. (2021). Rapid assessment of tsunami offshore propagation and inundation with D-FLOW flexible mesh and SFINCS for the 2011 Tōhoku Tsunami in Japan. *Journal of Marine Science and Engineering*, *9*(5), 453. https://doi.org/10.3390/jmse9050453
Sanders, B. F., & Schubert, J. E. (2019). PRIMo: Parallel raster inundation model. *Advances in Water Resources*, *126*(October 2018), 79–95. https://doi.org/10.1016/j.advwatres.2019.02.007
Santiago-Collazo, F. L., Bilskie, M. V., & Hagen, S. C. (2019). A comprehensive review of compound inundation models in low-gradient coastal watersheds. *Environmental Modelling & Software*, *119*(June), 166–181. https://doi.org/10.1016/j.envsoft.2019.06.002
Savage, J. T. S., Pianosi, F., Bates, P., Freer, J., & Wagener, T. (2016). Quantifying the importance of spatial resolution and other factors through global sensitivity analysis of a flood inundation model. *Water Resources Research*, *52*(11), 9146–9163. https://doi.org/10.1002/2015WR018198
Schaefer, J. T. (1990). The critical Success Index as an indicator of warning skill. *Weather and Forecasting*, *5*(4), 570–575. https://doi.org/10.1175/1520-0434(1990)005<0570:TCSIAA>2.0.CO;2
Schubert, J. E., Mach, K. J., & Sanders, B. F. (2024). National-scale flood hazard data unfit for urban risk management. *Earth's Future*, *12*(7). https://doi.org/10.1029/2024EF004549
Schumann, G. J. P., Andreadis, K. M., & Bates, P. D. (2014). Downscaling coarse grid hydrodynamic model simulations over large domains. *Journal of Hydrology*, *508*, 289–298. https://doi.org/10.1016/j.jhydrol.2013.08.051
Schumann, G. J. P., & Bates, P. D. (2018). The need for a high-accuracy, open-access global DEM. *Frontiers in Earth Science*, *6*(December), 1–5. https://doi.org/10.3389/feart.2018.00225
Sebastian, A., Bader, D. J., Nederhoff, C. M., Leijnse, T. W. B., Bricker, J. D., & Aarninkhof, S. G. J. (2021). Hindcast of pluvial, fluvial, and coastal flood damage in Houston, Texas during Hurricane Harvey (2017) using SFINCS. *Natural Hazards*, *109*(3), 2343–2362. https://doi.org/10.1007/s11069-021-04922-3
Shen, Y., Morsy, M. M., Huxley, C., Tahvildari, N., & Goodall, J. L. (2019). Flood risk assessment and increased resilience for coastal urban watersheds under the combined impact of storm tide and heavy rainfall. *Journal of Hydrology*, *579*(September), 124159. https://doi.org/10.1016/j.jhydrol.2019.124159
Slater, L. J. (2016). To what extent have changes in channel capacity contributed to flood hazard trends in England and Wales? *Earth Surface Processes and Landforms*, *41*(8), 1115–1128. https://doi.org/10.1002/esp.3927
Soil Survey Staff. (2022). Gridded national soil Survey geographic (gNATSGO) database for the conterminous United States. Retrieved from https://nrcs.app.box.com/v/soils
Sosa, J., Sampson, C., Smith, A., Neal, J., & Bates, P. (2020). A toolbox to quickly prepare flood inundation models for LISFLOOD-FP simulations. *Environmental Modelling & Software*, *123*(October 2019), 104561. https://doi.org/10.1016/j.envsoft.2019.104561
Stewart, S. R., & Berg, R. (2019). National hurricane center tropical cyclone Report: Hurricane florence (AL062018). Retrieved from https://www.nhc.noaa.gov/data/tcr/AL062018_Florence.pdf
Strauss, B. H., Orton, P. M., Bittermann, K., Buchanan, M. K., Gilford, D. M., Kopp, R. E., et al. (2021). Economic damages from Hurricane Sandy attributable to sea level rise caused by anthropogenic climate change. *Nature Communications*, *12*(1), 2720. https://doi.org/10.1038/s41467-021-22838-1
Thomson, H., Zeff, H. B., Kleiman, R., Sebastian, A., & Characklis, G. W. (2023). Systemic financial risk arising from residential flood losses. *Earth's Future*, *11*(4). https://doi.org/10.1029/2022EF003206
Titley, H. A., Cloke, H. L., Harrigan, S., Pappenberger, F., Prudhomme, C., Robbins, J. C., et al. (2021). Key factors influencing the severity of fluvial flood hazard from tropical cyclones. *Journal of Hydrometeorology*, *22*(7), 1801–1817. https://doi.org/10.1175/JHM-D-20-0250.1
Torres, J. M., Bass, B., Irza, N., Fang, Z., Proft, J., Dawson, C., et al. (2015). Characterizing the hydraulic interactions of hurricane storm surge and rainfall-runoff for the Houston-Galveston region. *Coastal Engineering*, *106*, 7–19. https://doi.org/10.1016/j.coastaleng.2015.09.004
Trigg, M. A., Birch, C. E., Neal, J. C., Bates, P. D., Smith, A., Sampson, C. C., et al. (2016). The credibility challenge for global fluvial flood risk analysis. *Environmental Research Letters*, *11*(9), 094014. https://doi.org/10.1088/1748-9326/11/9/094014
USACE. (2024a). National levee database. Retrieved from https://levees.sec.usace.army.mil/
USACE. (2024b). National structure inventory. Retrieved from https://www.hec.usace.army.mil/confluence/nsi
USDA-NRCS. (2004). Part 630 hydrology national engineering handbook: Hydrologic soil-cover complexes. Retrieved from https://irrigationtoolbox.com/NEH/Part630_Hydrology/H_210_630_09.pdf
USGS. (2024a). USGS flood event viewer. Retrieved from https://stn.wim.usgs.gov/FEV/
USGS. (2024b). USGS national map download. Retrieved from https://apps.nationalmap.gov/downloader/
USGS. (2024c). USGS national water dashboard. Retrieved from https://dashboard.waterdata.usgs.gov/app/nwd/en/?aoi=default
Van Oosterhout, L., Koks, E., Van Beukering, P., Schep, S., Tiggeloven, T., Van Manen, S., et al. (2023). An integrated assessment of climate change impacts and implications on Bonaire. *Economics of Disasters and Climate Change*, *7*(2), 147–178. https://doi.org/10.1007/s41885-023-00127-z
Van Ormondt, M., Leijnse, T., Nederhoff, K., De Goede, R., & Van Dongeren, A. (2023). SFINCS: Super-fast INundation of CoastS model (v2.0.2 Blockhaus release Q2 2023. *Zenodo*. https://doi.org/10.5281/zenodo.8038565
Volp, N. D., Van Prooijen, B. C., & Stelling, G. S. (2013). A finite volume approach for shallow water flow accounting for high-resolution bathymetry and roughness data. *Water Resources Research*, *49*(7), 4126–4135. https://doi.org/10.1002/wrcr.20324

Wing, O. E. J., Bates, P. D., Sampson, C. C., Smith, A. M., Johnson, K. A., & Erickson, T. A. (2017). Validation of a 30 m resolution flood hazard model of the conterminous United States. *Water Resources Research*, *53*(9), 7968–7986. https://doi.org/10.1002/2017WR020917

Wing, O. E. J., Pinter, N., Bates, P. D., & Kousky, C. (2020). New insights into US flood vulnerability revealed from flood insurance big data. *Nature Communications*, *11*(1), 1444. https://doi.org/10.1038/s41467-020-15264-2

Wing, O. E. J., Smith, A. M., Marston, M. L., Porter, J. R., Amodeo, M. F., Sampson, C. C., & Bates, P. D. (2021). Simulating historical flood events at the continental scale: Observational validation of a large-scale hydrodynamic model. *Natural Hazards and Earth System Sciences*, *21*(2), 559–575. https://doi.org/10.5194/nhess-21-559-2021

Woodrow, K., Lindsay, J. B., & Berg, A. A. (2016). Evaluating DEM conditioning techniques, elevation source data, and grid resolution for field-scale hydrological parameter extraction. *Journal of Hydrology*, *540*, 1022–1029. https://doi.org/10.1016/j.jhydrol.2016.07.018

Xu, H., Tian, Z., Sun, L., Ye, Q., Ragno, E., Bricker, J., et al. (2022). Compound flood impact of water level and rainfall during tropical cyclone periods in a coastal city: The case of Shanghai. *Natural Hazards and Earth System Sciences*, *22*(7), 2347–2358. https://doi.org/10.5194/nhess-22-2347-2022

Yankovsky, A. E., Torres, R., Torres-Garcia, L. M., & Jeon, K. (2012). Interaction of tidal and fluvial processes in the transition zone of the Santee river, SC, USA. *Estuaries and Coasts*, *35*(6), 1500–1509. https://doi.org/10.1007/s12237-012-9535-6

Ye, F., Huang, W., Zhang, Y. J., Moghimi, S., Myers, E., Pe'eri, S., & Yu, H.-C. (2021). A cross-scale study for compound flooding processes during Hurricane Florence. *Natural Hazards and Earth System Sciences*, *21*(6), 1703–1719. https://doi.org/10.5194/nhess-21-1703-2021

Zhang, Y. J., Ye, F., Yu, H., Sun, W., Moghimi, S., Myers, E., et al. (2020). Simulating compound flooding events in a hurricane. *Ocean Dynamics*, *70*(5), 621–640. https://doi.org/10.1007/s10236-020-01351-x

Erratum

The originally published version of this article contained a typographical error. In the first sentence of the first paragraph of the Introduction, "Tropical Cyclohnes" has been corrected to "Tropical Cyclones." This may be considered the authoritative version of record.